PROBING THE ACTIVE CONFORMERS OF PARAOXON THROUGH THEORETICAL CONFORMATIONAL STUDIES

Jason FORD-GREEN[1], Devashis MAJUMDAR[2] and Jerzy LESZCZYNSKI[3,*]

Department of Chemistry, Jackson State University, Jackson, MS 39217, U.S.A.;
e-mail: [1] jgreen@ccmsi.us, [2] devashis@ccmsi.us, [3] jerzy@ccmsi.us

Received May 4, 2008
Accepted July 10, 2008
Published online October 6, 2008

Dedicated to Professor Rudolf Zahradník on the occasion of his 80th birthday.

Theoretical conformational studies have been carried out at the density functional (DFT) level of theory on paraoxon (*O*,*O*-diethyl-*O*-*p*-nitrophenylphosphonate) to correlate its conformational and enzyme inhibition properties. The aqueous solvation of the various conformers has been studied at the DFT level using polarized continuum model with conductor-like solvation approach. The results show that paraoxon has high conformational flexibility in aqueous medium, although in gas phase the molecule is less flexible. The barriers to transition to different low-energy conformers in aqueous medium are thermally accessible. The molecular electrostatic potential surfaces of the various low-energy conformers of this molecule have been compared with the related enzyme-bound organophosphorus structures to investigate the role of the calculated conformers on the biological activity of this molecule.
Keywords: Paraoxon; Diethyl-4-methylbenzylphosphonate; Phosphotriesterase; AeCXE1 inhibitors; B3LYP functional; MEP; Conformation analysis; DFT calculations.

Paraoxon (*O*,*O*-diethyl-*O*-*p*-nitrophenylphosphate) is an acetylcholinesterase (AChE) inhibitor. This organophosphorus (OP) compound is the active metabolite of the insecticide parathion (*O*,*O*-diethyl-*O*-*p*-nitrophenylphosphorothiolate). In fact, the metabolic activation of parathion in mammals involves CYP450-mediated oxidative desulfuration to paraoxon (PO) and subsequent detoxification by CYP450-mediated dearylation to produce the major metabolite *p*-nitrophenol[1–3]. PO is electrophilic in character and phosphorylate the serine hydroxyl group located in the active site of AChE. The balance between desulfuration of parathion and dearylation of PO can result in very different level of AChE inhibition[4].

The nature of PO binding to AchE [4,5] has prompted several experimental and theoretical studies involving their complexes with plant carboxyl-

Collect. Czech. Chem. Commun. 2008, Vol. 73, No. 10, pp. 1245–1260

doi:10.1135/cccc20081245

esterase[6] (AeCXE1) and phosphotriesterase[7–9] (PTE). Earlier research on animal carboxylesterases has led to the classification of such enzymes in four different classes depending on their nature of interactions with OP compounds[10,11]. According to this classification, PTE belongs to the group of enzymes, which are inhibited by OP while AeCXE1 belongs to the class where OP is hydrolyzed. In the case of AeCXE1, OP molecules act as substrate through binding with the serine residue inside the active cavity of the enzyme. On the other hand, in the case of PTE enzyme, the OP inhibition mechanism involves its occupation of a site near the binuclear metal center (Zn) with the phosphoryl oxygen of the substrate situated at ~3.5 Å from the solvent exposed zinc ions[7–9]. In fact PO (or their inhibitors) is used as a substrate for such enzymes to model their active site[6,7]. The PTE from pseudomonas diminuta catalyzes the hydrolysis of PO with a very high turnover number[12]. The crystallographic studies of the interaction of PTE with diethyl-4-methylbenzylphosphonate (DEMBP, a typical inhibitor, closely related to PO)[7] generated a reliable description of the orientation of the substrate inside the active cavity – although the hydrolysis mechanism proposed by the authors needed modification from recent theoretical observations[8,9]. The crystallographic studies on the interaction of AeCXE1 with PO [6], on the other hand, has indicated that this OP molecule binds covalently to the active serine site, Ser-169, through the phosphate group. The binding mimics the first tetrahedral intermediate of the carboxylesterase reaction mechanism.

The understanding of the conformational aspects of PO in gas phase (low dielectric medium) as well as in aqueous medium (high dielectric medium) is quite important to understand its carboxylesterase inhibition property. The connection comes from the structural nature of the PTE/AeCXE1 active site[6,7]. The X-ray crystallographic studies characterize the active sites of these enzymes as narrow gorge composed of several amino acid residues. Thus, when PO enters the gorge for inhibition reaction, it will experience a dielectric change in the medium. Since the conformational properties of a solute are strongly affected by the change of dielectric constant of the medium, this effect will naturally have an influence in controlling the biological activity of PO. Moreover, the conformational properties of PO, responsible for the inhibition of such enzymes, could be used to interpret their activity towards cholinesterase (AChE) inhibition.

In view of the less available information on the conformational properties of PO connecting their biological activities, we have carried out *ab initio* quantum mechanical calculations of the rotational barriers and conformational equilibrium in this molecule. The conformational studies

have been carried out at the density functional (DFT)[13] level of theory. The hydration effect on the different conformers is taken into account through the polarized continuum calculations using conductor-like solvation (CPCM) model[14] at the DFT level. The present theoretical investigations involve the quantum mechanical evaluation of the thermodynamic properties and barriers for the conformational transitions of the molecule so that the feasibility of occurrence of a particular conformer could be understood. We have generated the molecular electrostatic potential (MEP) surfaces of the various low-energy conformers of this molecule and compared them with the PTE/AeCXE1 inhibitor-bound structures to find the role of the calculated conformers on the biological activity of this molecule.

METHODS OF COMPUTATION

Figure 1A shows the structure of PO. The structure indicates that the torsions governing the potential energy surface (PES) of this molecule are more than two (τ_1, τ_2, τ_3, τ_4, τ_5 and τ_6). Thus straightforward geometry optimization will not be able to locate the probable local minima of this molecule on the PES.

In order to locate the local and global minima, the (τ_1, τ_2) sections of the gas-phase PESs of PO were initially mapped by partial geometry optimization, in which the torsion angles τ_1 and τ_2 were kept constant and other degrees of freedom were relaxed. In these calculations, τ_1, and τ_2 were varied in 60° intervals. The low-energy geometries were calculated by full geometry optimizations started from the structures selected on the basis of PES. The partial and full geometry optimizations were carried out at the DFT level. The DFT calculations have used Becke's three-parameter functional[15] together with the local correlation part by Vosko et al.[16] and the non-local part by Lee, Yang and Parr[17] (in short B3LYP). The nature of the stationary points has been evaluated by subsequent calculation of harmonic vibrational frequencies. The rotational transition states connecting two low-energy conformers have been calculated using quadratic synchronous transit (QST2) method[18] at the DFT/B3LYP level and are characterized by single imaginary frequency.

Solvation free energies (ΔG_{solv}) were calculated at the DFT/B3LYP level using CPCM model[14]. The ΔG_{solv} values were calculated in aqueous continuum (ε = 78.39) and the molecular cavities were built using the UAHF (united atom for the Hartree–Fock) procedure, as used in CPCM. In principle, the free energy surfaces are determined by rigorous combination of free energy perturbation/umbrella sampling approaches[19,20]. These surfaces are

very rigorous as they reflect non-equilibrium solvation. However, such calculations are very challenging when performed within *ab initio* framework. Thus a more practical simplified approach has been adopted in our study. The relative free energies (ΔG) are determined as[21]

$$\Delta G = \Delta H_{\mathrm{gas}}^{298} - T\Delta S - RT \ln \omega + \Delta\Delta G_{\mathrm{solv}} \approx \Delta G_{\mathrm{gas}}^{298} + \Delta\Delta G_{\mathrm{solv}} \,. \qquad (1)$$

In Eq. (*1*), $\Delta H_{\mathrm{gas}}^{298}$ is enthalpy at 298 K, ΔS is the gas-phase entropy, $\Delta G_{\mathrm{gas}}^{298}$ is the Gibbs free energy at 298 K and $\Delta\Delta G_{\mathrm{solv}}$ is the relative free energy of solvation. The contribution of the term $RT \ln \omega$ is zero, as the electronic degeneracy term, ω, for the singlet state is unity. The ΔG values are used to calculate the relative population of various conformers of PO in aqueous medium.

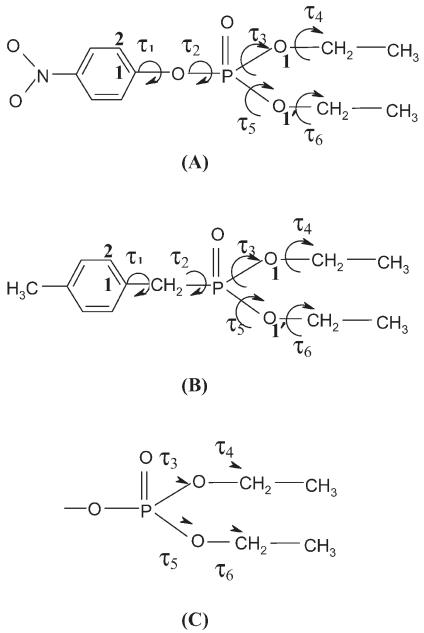

FIG. 1
Schematic representations of the structures of paraoxon (A), DEMBP (B), and DEP-fragment (C) indicating different torsion angles (τ_i). The torsion angles of DEP are defined in such a way that they could be compared directly with paraoxon

Since the molecules are much more floppy in solution than in the gas phase, we have used another definition of free energy (Δg_{flex}) to compare the intrinsic flexibility of different conformers, when embedded in aqueous medium. This is the practical implementation of the more general expression used by Warshel and coworkers[21,22]. The Δg_{flex} could be expressed as

$$\Delta g_{flex} = \Delta E_{solute} + \Delta ZPE + \Delta\Delta G_{solv} - \alpha T\Delta S \ . \qquad (2)$$

The ΔE_{solute} and ΔZPE in Eq. (*2*) are the relative gas-phase energy separations and the zero-point energies of the various conformers. The scale factor α is usually taken as zero[22] and the expression (*2*) could be simplified as

$$\Delta g_{flex} = \Delta H^{0}_{gas} + \Delta\Delta G_{solv} \ . \qquad (3)$$

All the terms in Eqs (*1*) and (*3*) are available from the thermochemical analyses based on statistical mechanics expressions utilizing the ideal gas, rigid rotator, and harmonic oscillator approximations[23].

The electrostatic properties of the various low-energy conformers of PO have been compared using the molecular electrostatic potential (MEP) surfaces generated on the isodensity surfaces of the respective conformers. The generated MEP surfaces have been also compared with the MEP surfaces of DEMBP (Fig. 1B) bound inside the cavity of PTE. The MEP surfaces of the cavities of PTE and AeCXE1 were also generated from their respective crystal structures and used to find the probable nature of electrostatic fit of the low-energy conformers of PO inside the cavity.

The calculations have been carried out at the 6-31++G(d,p) basis set level using Gaussian03 code[24]. The molecular graphics and the MEP surfaces have been generated using GaussView [25] and MOLEKEL [26,27] softwares, respectively.

RESULTS AND DISCUSSION

Conformation of Paraoxon

The results of energy calculations on different low-energy conformers of paraoxon are presented in Table I (DFT/B3LYP level). The conformational properties of paraoxon are oriented around the six torsion angles as depicted in Fig. 1A. The torsion angles τ_1 and τ_2 control the orientation of the nitrobenzene ring with respect to the P atom while the τ_3, τ_4, τ_5, and τ_6 con-

trol the orientation of the two ethoxy groups with respect to the P atom. Thus all of these six dihedral angles are needed to define a biologically active paraoxon conformer. For simplicity we have termed the low energy conformers in terms of the torsion angles τ_1 and τ_2 (Table I) and the orientation of these torsion angles is further characterized as gauche (*g*), eclipsed (*e*) and trans (*t*). This convention has been used throughout the paper. The torsion angles τ_i (i = 1–6) corresponding to all the low-energy conformers of paraoxon are available in Table II. The energetics and the important geometric features (in terms τ_i, i = 1–6) of the calculated transition states, connecting the conversion of the different low-energy conformers, are shown in Tables I and II, respectively.

The gas-phase results (in terms of ΔH^0_{gas}, Table I) show that there are six possible low-energy conformers of paraoxon and three of them are within 1 kcal/mol energy separation. The lowest energy conformer is g^-t. Figure 2 shows the energy profiles of the low-energy conformers of paraoxon. These

TABLE I

Calculated relative stabilities (kcal/mol) of the various low-energy conformers of paraoxon in the gas phase (DFT/B3LYP/6-31++G(d,p) level) and in aqueous medium. Calculated dipole moments (μ, D) of the various low-energy conformers in the gas phase are also included

Conformer (τ_1, τ_2)	ΔH^0_{gas} [b]	ΔH^{298} [c]	ΔG^{298} [c]	$\Delta\Delta G_{sol}$ [d]	ΔG [e]	Δg_{flex} [f]	μ
g^-t (–35.0, 175.4)	0.00	0.00	0.00	0.00	0.00	0.00	6.47
et (148.5, 175.4)	0.02	0.01	0.06	0.01	0.07	0.03	6.43
e^-g (–146.3, 75.3)	0.67	0.51	1.37	–0.21	1.16	0.46	4.73
gg (80.8, 35.9)	1.31	1.31	1.61	–0.80	0.82	0.52	6.50
e^-g^- (–16.1, –42.9)	1.76	1.78	1.82	–1.50	0.32	0.27	4.73
tg^- (164.8, –42.9)	1.76	1.78	1.81	–1.50	0.32	0.27	4.73
TS_1 ($tg^- \rightarrow g^-t$)	3.39	2.91	4.64	–1.08	3.56	2.31	–
TS_2 ($e^-g^- \rightarrow g^-t$)	3.42	2.96	4.25	–1.39	2.87	2.03	–
TS_3 ($g^-t \rightarrow gg$)	1.30	0.80	2.56	–0.59	1.97	0.71	–
TS_4 ($e^-g^- \rightarrow et$)	1.70	1.21	2.12	–0.28	1.84	1.42	–
TS_5 ($e^-g^- \rightarrow gg$)	1.60	1.01	2.92	–0.82	2.10	0.77	–

[a] Classification of stationary points are based on the gas-phase potential energy surface. Transition states are denoted by TS. [b] $\Delta H^0_{gas} = \Delta E_{gas} + \Delta ZPE$. [c] ΔH^{298} and ΔG^{298} are the relative gas-phase enthalpies and free energies at 298 K. [d] $\Delta\Delta G_{solv}$ is the relative solvation energy calculated at the B3LYP/CPCM level. [e] $\Delta G = \Delta G^{298} + \Delta\Delta G_{sol}$. [f] $\Delta g_{flex} = \Delta H^0_{gas} + \Delta\Delta G_{sol}$ (see the text for details).

TABLE II

Important geometric features[a] (torsion angles (τ, °) and bond distances (*r*, Å)) of the various low-energy conformers of paraoxon and the transition states (TS) connecting these conformers (DFT/B3LYP/6-31++G(d,p) level). Geometric features of DEMBP conformers (bound to the active cavity of PTE) and diethylphosphonate (DEP) fragment (bound to AeCXE1) are also presented for comparison

Molecule	Conformers/ TS[d]	τ_1	τ_2[e]	τ_3	τ_4	τ_5	τ_6	$r(C_1–O)$/ $r(C_1–C)$[f]	r(O–P)/ r(C–P)[f]
Paraoxon	g^-t	–35.0	175.4 (–79.0)	–83.6	–166.7	168.9	–166.7	1.384	1.63
	et	147.7	175.6 (–78.7)	–83.4	–166.1	168.1	–163.1	1.384	1.63
	e^-g	–146.3	75.3 (–178.5)	–162.2	–91.5	90.8	–93.3	1.378	1.628
	gg	35.5	81.0 (–173.4)	107.3	–154.5	177	–171.9	1.381	1.629
	e^-g^-	–16.1	–42.9 (–62.8)	–86.3	–162.8	168.9	–170.5	1.378	1.628
	tg^-	164.8	–42.9 (62.9)	–86.3	–162.8	168.9	–170.5	1.378	1.628
	TS_1	67.0	–9.4 (–115.4)	–87.1	–165.7	167.8	–169.3	1.381	1.629
	TS_2	–67.8	–0.8 (–106.5)	–88.2	–165.7	176.9	–174.1	1.381	1.628
	TS_3	23.6	105.7 (–149.6)	–94.8	–164.5	–179.6	–172.6	1.381	1.629
	TS_4	41.4	68.7 (174.9)	–114.3	–157.2	130.6	–123.7	1.381	1.636
	TS_5	44.5	175.3 (66.6)	–141.4	–157.2	130.6	–123.7	1.381	1.636
DEMBP[b]	1	–78.8	–67.6 (35.6)	–131.2	–142.7	112.0	155.3	1.533	1.612
	2	–93.7	–59.9 (49.4)	126.0	144.7	94.6	–170.5	1.535	1.620
	3	–92.8	–70.7 (35.0)	–39.3	–127.2	164.5	–101.3	1.520	1.608
	4	–80.0	–71.3 (35.6)	–45.8	–107.0	164.4	111.2	1.540	1.601
DEP[c]		–	–	131.2	–124.9	176.9	156.1	–	1.787

[a] Refer to Fig. 1 for the definition of the geometric parameters. [b] Ref.[7] [c] Ref.[6] [d] Refer to Table I for the definition of the TS. [e] The τ_2 values within parentheses refer to the torsion angle using $O_{1'}$ (refer to Fig. 1 for definition of atom numberings). [f] The parameters specify distances in DEMBP conformers (Fig. 1B).

low-energy conformers are connected through transition states (Fig. 2, Table I) with energy barriers within 4.0 kcal/mol. This indicates that the transitions between the various low-energy conformers of paraoxon are thermally allowed in the gas phase.

The *et* and $e^{-}g$ conformers have very small energy separation with respect to the minimum energy conformer ($g^{-}t$). The three other conformers, viz., *gg*, $e^{-}g^{-}$, and tg^{-} are quite high-energy conformers in the gas phase (Table I). The calculation of ΔG^{298} values (Table I) shows that the free energy separations of these conformers are further increased and only $g^{-}t$ and *et* could be the feasible conformers in the gas phase. As it could be seen from Table II, the nitro group at the para position creates a slight shortening of the C_1–O bond length (due to conjugation) with respect to the standard single C–O bond length (1.43 Å). This causes restriction in the τ_1 rotation and consequently a few low-energy conformers are feasible in the gas phase.

The low-energy conformers of paraoxon have quite high dipole moments and as a result, they are expected to be solvated in aqueous medium. The calculated relative free energy of solvation ($\Delta\Delta G_{solv}$) contributes quite significantly towards the free energy separations (ΔG, Table I) of the conformers

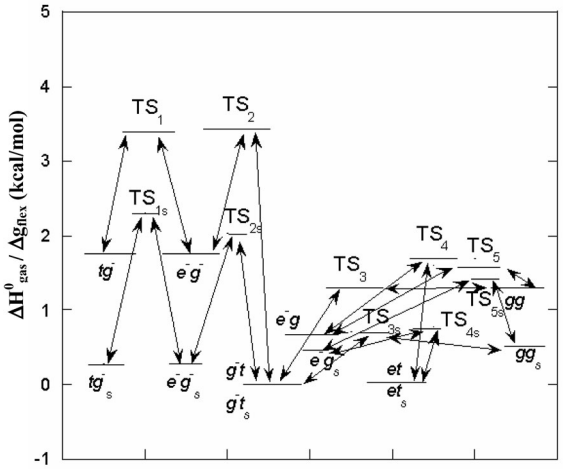

FIG. 2

Calculated energy profiles are presented for the transformations of the various low-energy conformers of paraoxon in the gas phase (in terms of $\Delta H_{gas}{}^{0}$) and in aqueous continuum (in terms of Δg_{flex}). The conformers and the transition states (TS) are subscripted with 's' for the energy profiles due to aqueous solvation

in the aqueous medium and several low-energy conformers are finitely populated because of the low ΔG (ΔG^{298} + $\Delta\Delta G_{solv}$) separation with respect to the global minimum energy conformer (g^-t). Although the dipole moment values of the different conformers show that they are soluble in aqueous medium, the magnitudes of $\Delta\Delta G_{solv}$ in CPCM model are dependent on the solvation charges, and total electrostatic potential generated by the solute nuclei and electrons[14]. The nonelectrostatic interaction energy parameters, viz., cavitation, dispersion and repulsion, also contribute significantly towards $\Delta\Delta G_{solv}$ term[14,28]. In the case of paraoxon conformers the nonelectrostatic contribution towards $\Delta\Delta G_{solv}$ does not differ much, but the electrostatic contributions are higher for the conformers with higher energy separations in the gas phase. As a result the calculated ΔG (ΔG^{298} + $\Delta\Delta G_{solv}$) (Table I) and Δg_{flex} show reduced energy separation between the conformers due to aqueous solvation. It is to be mentioned in this connection that the uncertainty in the estimation of ΔG (and Δg_{flex}) is ~0.7 kcal/mol [22] and thus for conformers with very low-energy separations (which is also the case of paraoxon), the results should be treated in a qualitative sense.

Figure 2 also represents the Δg_{flex} profiles for the transitions of the various low-energy conformers in aqueous medium. The highest barrier for $tg^- \leftrightarrow g^-t$ transition (TS_1) as determined by the relative free energy (ΔG^{298}) of TS_1 structure is 4.64 kcal/mol in the gas phase. This barrier reduces to 2.31 kcal/mol during aqueous solvation. The Δg_{flex} and ΔG values of the transition states (Table I) indicate that the barrier heights of all the transitions between different conformers are, in fact, decreased due to solvation. These barriers are thermally accessible and the transitions between the different low-energy conformers of paraoxon are feasible in aqueous medium.

Effect of the Low-Energy Conformers on the Biological Activity

It is generally believed that the substrates inside the enzyme cavity does not usually retain its lowest energy conformation during binding and adapts a shape, which is feasible for such binding. Questions may then arise regarding the justification of studying the low-energy conformers of paraoxon to interpret its biological activity. While entering the cavity, the substrate definitely remains in its low-energy conformational space (depending on the dielectric of the medium). It adopts a specific active conformation during the binding process. Thus for most of the cases, the role of the low-energy conformers of a substrate in correlating biological activity lies in the feasibility of generating the active conformer[29,30]. If a particular low-energy conformer is itself the active one, then, of course, the correlation is more

direct[31]. The simplest way to analyze the nature of such active conformer(s) of paraoxon is to compare enzyme-bound substrate (paraoxon or its inhibitor) conformation with the low-energy conformers of paraoxon. The present section will represent such comparisons using the crystal structure data of PTE...DEMBP [7] and AeCXE1...paraoxon[6] complexes.

Comparison of the paraoxon conformers with PTE bound DEMBP. The crystal structure of PTE bound DEMBP has been investigated at the pre-hydrolysis stage of the inhibitor[7]. Since DEMBP has close structural relationship with PO, it is worthwhile to compare their conformational topology to get an idea of the active conformation(s) of PO. Four different conformers of DEMBP (Fig. 1B) could be located in the crystal of this PTE bound inhibitor[7]. These conformers are marked as 1, 2, 3, 4, and their important geometric features are shown in Table II. The four active DEMBP conformers have some structural similarities with PO conformers regarding the orientation of the phosphonate and the two ethyl groups. The orientation of the methyl-benzyl part of DEMBP is not expected to show any similarity with the *O-p*-nitrophenyl part of PO. The similarity is also not that vital as they are the leaving groups during enzymatic hydrolysis. It is only important to investigate whether the aromatic part of any low-energy conformer of PO, like the aromatic part of DEMBP [7], could be accommodated inside the active cavity of PTE with electrostatic complementarity of the MEP surfaces.

The comparison of structural similarities between the different conformers could be carried out in a more efficient way through direct comparison of their molecular topology and MEP surfaces. Figure 3 shows the comparison of the MEP surface topology of the low-energy conformers of paraoxon (g^-t, *gg*, e^-g^-, and tg^-) with DEMBP-1 and DEMBP-2 (DFT/B3LYP/6-31++(d,p) level). Our detailed structural topology analyses have indicated that g^-t and *gg* conformers of paraoxon show similar structural topology with DEMBP-1 regarding the orientations of the phosphonate and the two ethyl groups. The e^-g^-, and tg^- conformers bear similar relationship with DEMBP-2 in this regard. The MEP surface comparisons, as shown in Fig. 3, are based on the observations of molecular topology comparison. The MEP surfaces of the respective conformers have been compared by keeping them at the same relative orientations as obtained from molecular topology analyses, and it could be observed that the g^-t and *gg* conformers of paraoxon correlates with DEMBP-1 quite well. The topology of the MEP surfaces of the e^-g^- and tg^- conformers also matches with DEMBP-2 but the correlation is not as good as in the case of DEMBP-1. The striking feature of such analyses is that we are locating the active conformers of paraoxon, which are related to each other through low transition barrier in aqueous medium. Thus these

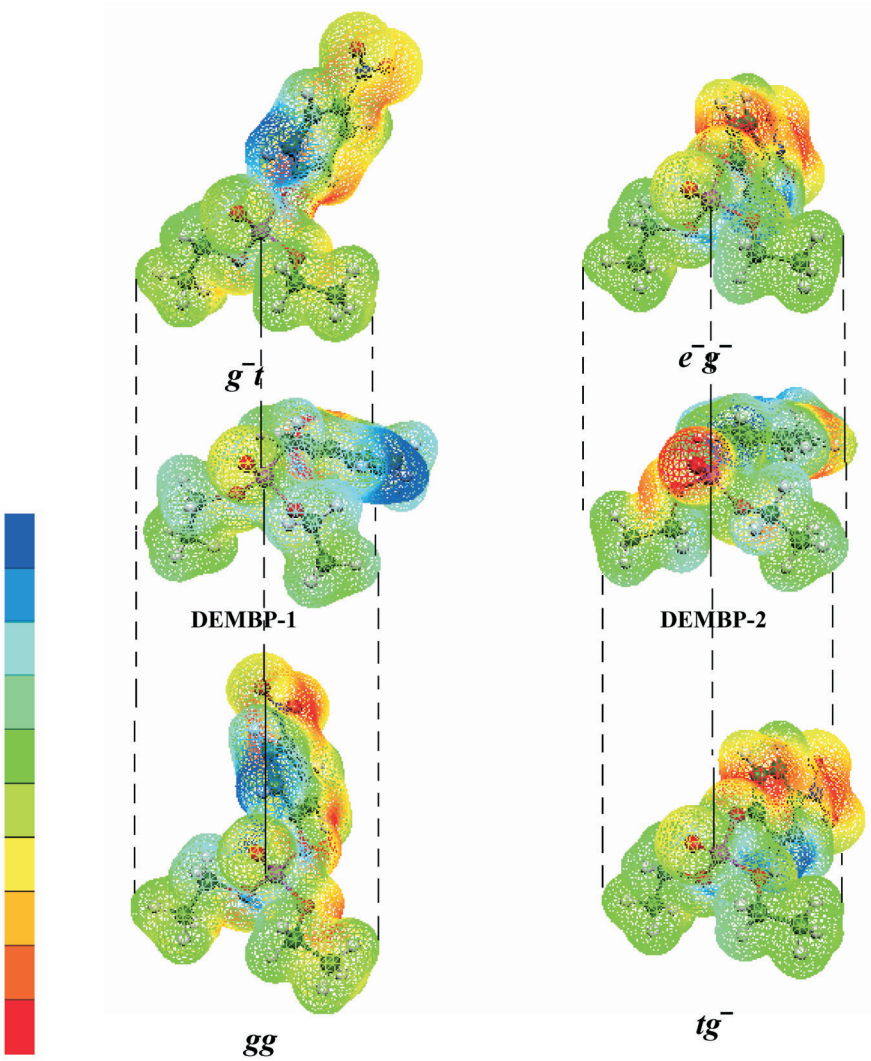

FIG. 3

Comparison of the topology of the calculated MEP on the isodensity surfaces of paraoxon conformers (g^-t, gg, e^-g^-, and tg^-) with those of DEMBP-1 and DEMBP-2. The surfaces are drawn from a maximum of 144.0 kcal/mol (blue region) to a minimum of –100.0 kcal/mol (red region). The different colored regions are drawn at an interval of ~24 kcal/mol and the color transitions representing sift in magnitude of the MEP contour are according to the order of the color chart as indicated in the picture

active conformers, if different from g^-t conformer, could be generated from this minimum energy (g^-t) conformer.

A further in-depth analysis, in this respect, has been carried out by comparing the MEP surfaces of DEMBP and the low-energy conformers of paraoxon bound inside the active cavity of PTE. Figure 4A represents the MEP surface of the active cavity of PTE. The MEP surface has been derived from the crystal structure of PTE (active cavity)...DEMBP complex as shown in Fig. 4B. The active cavity of PTE contains several amino acid residues, viz., His-55, His-57, Trp-131, His-201, His-230, Asp-232, Asp-233, Asp-254, His-257, Leu-271, Asp-301, Phe-306, Tyr-309, Met-317 (ref.[7]). The main atoms of these amino acid residues are terminated by hydrogen atoms to neutralize the excess charges. The relevant MEP surfaces have been generated using DFT/B3LYP/3-21G* wave functions. Figure 4C represents the MEP surface of the active cavity of PTE with g^-t conformer of paraoxon placed inside the cavity. The orientation of this paraoxon conformer has been adjusted using the information from Figs 3 and 4B. This comparison is qualitative but it reveals similar topological features of the PTE bound inhibitor (Fig. 4A). The electrostatic complementarity of the aromatic part of PO conformer (g^-t) with those of the hydrophobic part of the cavity further shows that the low-energy conformers of paraoxon could be accommodated inside the active cavity at the pre-hydrolysis stage, and thus ascertaining their role as active conformers.

Comparison of the paraoxon conformers with AeCXE1 bound paraoxon. The crystal structure of AeCXE1 bound paraoxon[6] shows that the inhibitor is already hydrolyzed and the *O*-*p*-nitrobenzene part is released as *p*-nitrophenol. The diethylphosphonate (DEP) moiety is only residing within the active cavity of AeCXE1 through bonding with Ser-169. Thus, one can only compare the orientation of the phosphonate and the ethyl groups of the bound complex with those of the different low-energy conformers of paraoxon, but it would generate only partial information about the active paraoxon conformer. Table II contains the important geometric features of the DEP moiety (Fig. 2C) of the AeCXE1 bound complex[6] and it shows that the *gg* conformer of paraoxon has conformational similarity with this fragment regarding the orientation of phosphonate and ethyl groups (from τ_i values, i = 3–6, Fig. 1C). The lowest energy conformer (g^-t) of paraoxon does not show full compatibility with bound fragment from such τ-value considerations. A further investigation on the MEP surfaces has been carried out to ascertain the validity of such structural topology analysis.

Figure 5A shows the MEP surface (DFT/B3LYP/3-21G* level) of the active cavity of AeCXE1 bond with DEP. The active cavity of AeCXE1 contains

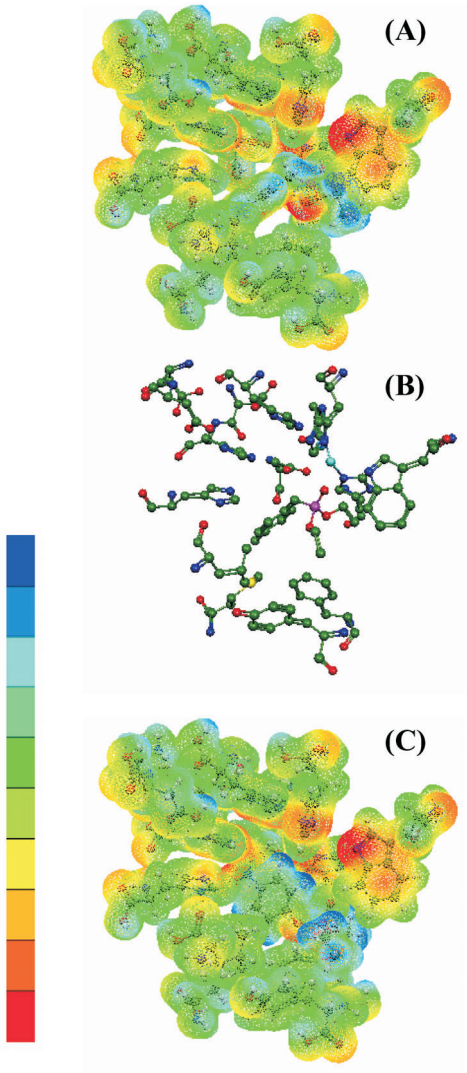

FIG. 4
Comparison of the topology of the calculated MEP on the isodensity surfaces of DEMBP-1 (A) and paraoxon ($g^{-}t$ conformer) (C) bound inside active cavity of PTE. Figure 4B represents the molecular structure of DEMBP-1 bound PTE from the crystallographic coordinates. See the text inside for the details of amino acid sequences and the way of generating the MEP surfaces for comparison of their topology. The MEP surfaces are drawn from a maximum of 55.0 kcal/mol (blue region) to a minimum of –74 kcal/mol (red region). The different colored regions are drawn at an interval of ~13.0 kcal/mol and the color transitions representing sift in magnitude of the MEP contour are according to the order of the color chart as indicated in the picture

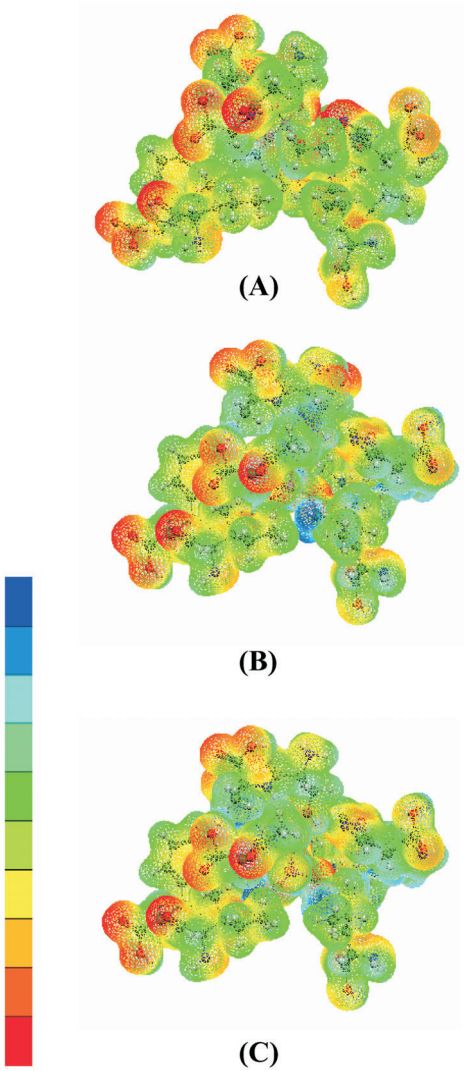

FIG. 5

Comparison of the topology of the calculated MEP on the isodensity surfaces of DEP fragment (bound to Ser-169 after paraoxon hydrolysis) (A), $g^{-}t$ (B) and *gg* conformers of paraoxon (C) bound inside active cavity of AeCXE1. See the text inside for the details of amino acid sequences and the way of generating the MEP surfaces for comparison of their topology. The MEP surfaces are drawn from a maximum of 55.0 kcal/mol (blue region) to a minimum of –74 kcal/mol (red region). The different colored regions are drawn at an interval of ~13.0 kcal/mol and the color transitions representing sift in magnitude of the MEP contour are according to the order of the color chart as indicated in the picture

Gly-92, Gly-93, Ser-169, Ala-170, Leu-222, Ile-230, Trp-231, Asp-276, Met-278, His-306 amino acid residues[6]. The MEP surfaces of the active cavity of AeCXE1 (with and without DEP bound to Ser-169) have been generated by terminating the open main atom positions with hydrogen atoms. In Figs 5B and 5C, the $g^{-}t$ and *gg* conformers of paraoxon are placed inside the active cavity of AeCXE1 to generate the respective MEP surfaces (DFT/B3LYP/3-21G* level). The relative orientations of these conformers, with respect to that of DEP in Fig. 5A, have been obtained from information of the molecular topology analyses. The comparison of the Figs 5A and 5B shows that they have similar MEP surface topology and the $g^{-}t$ and *gg* fits inside the active of AeCXE1 with similar electrostatic complementarity (with the active cavity of AeCXE1) like the complex in Fig. 5A.

CONCLUSIONS

The conformational properties of PO have been studied at the DFT/B3LYP level in the gas phase as well as in aqueous medium to locate the low-energy conformers of this molecule and to find correlation of these conformers with the observed PTE and AeCXE1 inhibition properties of this molecule. Two low-energy conformers of paraoxon have been identified in the gas phase. In aqueous medium, the molecule is more flexible and four low-energy conformers with very low-energy separation have been located. The MEP studies have been conducted on the active cavity of PTE bound DEMBP (paraoxon inhibitor) and AeCXE1 bound PO (hydrolyzed form). A comparison of these MEP surfaces with those of the low-energy PO conformers indicates that the active conformers are related to the $g^{-}t$ and *gg* conformers. The results of these qualitative investigations could be used as a template to understand the nature of AchE inhibition by paraoxon, as the enzyme cavity of AchE has similar binding site for paraoxon (Ser-200) compared to AeCX1 (Ser-169). The AchE inhibition by paraoxon is the key factor for its toxicity in living organisms and we shall address this problem in near future.

This work was facilitated by the support of the NSF CREST (Grant No. HRD-0318519) and CMCM (ERDC) grants. We would like to thank the Mississippi Center for Supercomputing Research for a generous allotment of computer time.

REFERENCES

1. Sultatos L. G., Murphy S. D.: *Fundam. Appl. Toxicol.* **1983**, *3*, 16.
2. McCracken N. W., Blain P. G., William F. M.: *Biochem. Pharmacol.* **1993**, *45*, 31.
3. Poet T. S., Wu H., Kousba A., Timchalk C.: *Toxicol. Sci.* **2003**, *72*, 193.

4. Timchalk C., Nolan R. J., Mendrala A. L., Dittenber D. A., Brzak K. A., Mattson J. L.: *Toxicol. Sci.* **2002**, *66*, 34.
5. Kousba A. A., Sultatos L. G., Poet T. S., Timchalk C.: *Toxicol. Sci.* **2004**, *80*, 239.
6. Ileperuma N. R., Marshall S. D. G., Squire C. J., Baker H. M., Oakeshott J. G., Russell R. J., Plummer K. M., Newcomb R. D., Baker E. N.: *Biochemistry* **2007**, *46*, 1851.
7. Vanhooke J. L., Benning M. M., Raushel F. M., Holden H. M.: *Biochemistry* **1996**, *35*, 6020.
8. Wong K.-Y., Gao J.: *Biochemistry* **2007**, *46*, 13352.
9. Chen S.-L., Fang W.-H., Himo F.: *J. Phys. Chem. B* **2007**, *111*, 1253.
10. Aldrige W. N.: *Biochem. J.* **1953**, *53*, 110.
11. Walker C. H. in: *Enzyme Hydrolyzing Organophosphorus Compounds* (E. Reiner, W. N. Aldrige and F. C. G. Hoskin, Eds), p. 236. Ellis Horwood Ltd., New York 1989.
12. Dumas D. P. Cladwell S. R., Wild J. R., Raushel F. M.: *J. Biol. Chem.* **1989**, *264*, 19659.
13. Parr R. G., Wang W.: *Density Functional Theory of Atoms and Molecules*. Oxford University Press, Oxford, New York 1984.
14. Barone V., Cossi M.: *J. Phys. Chem. A* **1998**, *102*, 1995.
15. Becke A. D.: *J. Chem. Phys.* **1993**, *98*, 5648.
16. Vosko S. H., Wilk L., Nusair M.: *Can. J. Phys.* **1980**, *58*, 1200.
17. Lee C., Wang W., Parr R. G.: *Phys. Rev. B* **1988**, *37*, 785.
18. Peng C., Ayola P. Y., Schlegel H. B., Frisch M. J.: *J. Comput. Chem.* **1996**, *17*, 49.
19. Hwang J. K., King G., Creighton S., Warshel A.: *J. Am. Chem. Soc.* **1998**, *110*, 5267.
20. Warshel A.: *Computer Modeling of Chemical Reactions in Enzymes and Solutions*. John Wiley & Sons, New York 1991.
21. Florian J., Warshel A.: *J. Phys. Chem. B* **1998**, *102*, 719.
22. Florian J., Strajbl M., Warshel A.: *J. Am. Chem. Soc.* **1998**, *120*, 7959.
23. Davidson N.: *Statistical Mechanics*. McGraw–Hill, New York 1962.
24. Frisch M. J., Trucks G. W., Schlegel H. B., Scuseria G. E., Robb M. A., Cheeseman J. R., Montgomery J. A., Jr., Vreven T., Kudin K. N., Burant J. C., Millam J. M., Iyengar S. S., Tomasi J., Barone V., Mennucci B., Cossi M., Scalmani G., Rega N., Petersson G. A., Nakatsuji H., Hada M., Ehara M., Toyota K., Fukuda R., Hasegawa J., Ishida M., Nakajima T., Honda Y., Kitao O., Nakai H., Klene M., Li X., Knox J. E., Hratchian H. P., Cross J. B., Bakken V., Adamo C., Jaramillo J., Gomperts R., Stratmann R. E., Yazyev O., Austin A. J., Cammi R., Pomelli C., Ochterski J. W., Ayala P. Y., Morokuma K., Voth G. A., Salvador P., Dannenberg J. J., Zakrzewski V. G., Dapprich S., Daniels A. D., Strain M. C., Farkas O., Malick D. K., Rabuck A. D., Raghavachari K., Foresman J. B., Ortiz J. V., Cui Q., Baboul A. G., Clifford S., Cioslowski J., Stefanov B. B., Liu G., Liashenko A., Piskorz P., Komaromi I., Martin R. L., Fox D. J., Keith T., Al-Laham M. A., Peng C. Y., Nanayakkara A., Challacombe M., Gill P. M. W., Johnson B., Chen W., Wong M. W., Gonzalez C., Pople J. A.: *Gaussian03*, Revision C.02. Gaussian, Inc., Wallingford (CT) 2004.
25. *GaussView*. Commercial Molecular Graphics Software. Gaussian, Inc., Wallingford (CT) 2004.
26. Flükigerb P., Lüthi H. P., Portmann S.: *MOLEKEL 4.3*. J. Weber, Swiss Center for Scientific Computing, Manno, Switzerland 2000–2002.
27. Portmann S., Lüthi H. P.: *Chimia* **2000**, *54*, 766.
28. Tomasi J., Mennucci B., Cammi R.: *Chem. Rev.* **2005**, *105*, 2999.
29. Majumdar D., Roszak S., Leszczynski J.: *J. Phys. Chem. B* **2006**, *110*, 13597.
30. Majumdar D., Roszak S., Leszczynski J.: *Mol. Phys.* **2007**, *105*, 2551.
31. Paukku Y., Michalkova A., Majumdar D., Leszczynski J.: *Chem. Phys. Lett.* **2006**, *422*, 317.